Journal of Thermal Analysis and Calorimetry (2019) 135:357–369
https://doi.org/10.1007/s10973-018-7069-2

Marangoni natural convection in a cubical cavity filled with a nanofluid

Buongiorno's nanofluid model

Mikhail A. Sheremet[1] · Ioan Pop[2]

Received: 8 January 2018 / Accepted: 10 February 2018 / Published online: 20 February 2018

Abstract
Natural convection in a differentially heated cubical cavity filled with a water-based nanofluid under the Marangoni effect from the upper free surface is studied numerically. It is supposed that the Brownian diffusion and thermophoresis are the major slip mechanisms for nanoparticles. Dimensionless governing equations formulated using vector potential functions, vorticity vector and temperature have been solved by the finite difference method of the second-order accuracy. It should be noted that the Marangoni effect is owing to the dependences of surface tension on the temperature and nanoparticles concentration. The effects of the Marangoni number, Lewis number, buoyancy ratio parameter, Brownian diffusion parameter and thermophoresis parameter on nanofluid flow, heat and mass transfer have been analyzed. It has been revealed that a growth of Marangoni number results in the heat transfer rate reduction.

Keywords Natural convection · Free surface · Marangoni effect · Three-dimensional cavity · Nanofluids · Brownian motion · Thermophoresis · Numerical results

List of symbols

Roman letters

C	Nanoparticle volume fraction (−)
C_0	Characteristic nanoparticle volume fraction (−)
D_B	Brownian diffusion coefficient ($m^2\ s^{-1}$)
D_T	Thermophoretic diffusion coefficient ($m^2\ s^{-1}$)
$\mathbf{g}$	Gravitational acceleration vector ($m\ s^{-2}$)
$\mathbf{j}_p$	Nanoparticles mass flux ($kg\ m^{-2}\ s^{-1}$)
L	Size of the cavity (m)
Le	Lewis number (−)
Ma_C	Marangoni number due to concentration difference effect (−)
Ma_T	Marangoni number due to temperature difference effect (−)
Nb	Brownian diffusion parameter (−)
Nr	Buoyancy ratio parameter (−)
Nt	Thermophoresis parameter (−)
Nu	Local Nusselt number (−)
$\overline{Nu}$	Average Nusselt number (−)
p	Dimensional pressure ($kg\ m^{-1}\ s^{-2}$)
Pr	Prandtl number (−)
Ra	Rayleigh number (−)
t	Dimensional time (s)
T	Dimensional temperature (K)
T_c	Cooled temperature of the vertical surface at $\bar{x} = L$ (K)
T_h	Heated temperature of the vertical surface $\bar{x} = 0$ (K)
T_0	Mean temperature of the heated and cooled surfaces (K)
$\mathbf{V}$	Dimensional velocity vector ($m\ s^{-1}$)
$\bar{u}, \bar{v}, \bar{w}$	Dimensional velocity components ($m\ s^{-1}$)
x, y, z	Dimensionless Cartesian coordinates (−)
$\bar{x}, \bar{y}, \bar{z}$	Dimensional Cartesian coordinates (m)

Greek symbols

α	Thermal diffusivity ($m^2\ s^{-1}$)

✉ Mikhail A. Sheremet
Michael-sher@yandex.ru

[1] Laboratory on Convective Heat and Mass Transfer, Tomsk State University, Tomsk, Russia 634050

[2] Department of Mathematics, Babeş-Bolyai University, 400084 Cluj-Napoca, Romania

β	Volumetric expansion coefficient (K^{-1})
δ	Heat capacitance ratio (−)
θ	Dimensionless temperature (−)
μ	Dynamic viscosity (kg m^{-1} s^{-1})
ρ_{f0}	Fluid density (kg m^{-3})
ρ_p	Nanoparticle mass density (kg m^{-3})
σ	Surface tension (kg s^{-2})
ϕ	Nanoparticles volume fraction (−)
$\bar{\psi}_x$, $\bar{\psi}_y$, $\bar{\psi}_z$	Dimensional vector potential functions (m^2 s^{-1})
ψ_x, ψ_y, ψ_z	Dimensionless vector potential functions (−)
$\bar{\omega}_x$, $\bar{\omega}_y$, $\bar{\omega}_z$	Dimensional vorticity vector components (s^{-1})
ω_x, ω_y, ω_z	Dimensionless vorticity vector components (−)

Subscripts

c Cold
f Fluid
h Hot
p Nanoparticle

Introduction

It is known for many years that the local variation in solute concentration at the interface in liquid–liquid solvent extraction systems would cause local increase or decrease in interfacial tension and thus induce additional convection at the interface (so-called interfacial turbulence). If this convection is localized and segmented, it would often generate local flow patterns on the subdroplet scale, leading to convection in the direction normal to the interface. It in turn enhances inter-phase mass transfer. This phenomenon is known to chemical engineers as the Marangoni effect [1]. Quite diversified forms of phenomena in inter-phase mass transfer were altogether termed as the Marangoni effect, such as drop pulsation, localized eruption, kicking and surface rippling [2]. Theoretical studies of the Marangoni effect were mainly focused on the criteria to judge whether the Marangoni effect would occur for specific liquid–liquid or liquid–gas interfaces and also solid–liquid gradient that induces the flow systems [3–7]. The mechanism and prediction of the Marangoni effect is an important subject for most practical extraction systems in the fundamental research related to solvent extraction. Marangoni flows exhibit fascinating scientific phenomena with ramifications to variety of fields including microfluidic, extraction processes and flow of sap in the xylem of high trees, just to name a few (see Tadmor [8], who presented an excellent review paper on Marangoni effect).

Marangoni flow induced by surface tension along a liquid surface causes undesirable effects in crystal growth melts in the same manner as buoyancy-induced natural convection. These undesirable effects also occur in space-based crystal growth experiments since Marangoni flow occurs in microgravity as well as in earth gravity. The surface tension gradients that are responsible for Marangoni convection can be both temperature and/or concentration gradients [9]. It seems that the basic research work in this field was first promoted by Napolitano [10, 11]. As pointed out by Napolitano [12], the field equations in the bulk fluids do not depend explicitly on the geometry of the interface when using as coordinates the arc length (x). This, together with the other surface balance equations, introduces kinematic, thermal and pressure couplings for the flow fields in the two fluids. Similarity solutions for Marangoni boundary layers exist when the interface temperature gradient varies as a power of the interface arc length (x). Numerical solutions on Marangoni boundary layers were found, analyzed and discussed by many authors, e.g., the papers by Pop et al. [13], Chamkha et al. [14], Al-Mudhaf and Chamkha [15] and Arifin et al. [16].

Transitions of Rayleigh–Bénard convection from the laminar to turbulence regime in small cavities have been studied extensively both experimentally and numerically [17–21]. Many routes to turbulence have been identified. Rahal et al. [22] have made an experimental study for the transition in Bénard–Marangoni convection in a cavity, where the temperature gradients are in the vertical direction. Transitions in cavities with horizontal temperature gradient have also been investigated, with pure buoyancy effect by Bucchignani and Mansutti [23, 24]. We mention also the paper by Li et al. [25] on double-diffusive Marangoni convection in a rectangular cavity. A similarly special and of equal importance case where the driven mechanism is surface tension rather than buoyancy was first considered by Bergman [26]. In this double-diffusive Marangoni convection where the thermal and solutal Marangoni effects due to horizontal temperature and concentration gradients are equal and opposing, the pure conductive equilibrium solution can remain stable up to a critical Marangoni number, beyond which convection happens. Also Chamkha [27] studied unsteady, laminar double-diffusive convective flow of a binary gas mixture in a rectangular porous cavity. A temperature-dependent heat source or sink is assumed to exist within the enclosure boundaries. It was found that the heat and mass transfer and the flow characteristics inside the cavity depended strongly on the inverse Darcy number and the heat generation or absorption effects. Chamkha et al. [28] examined laminar free convection of a micropolar fluid in a vertical parallel plate channel with asymmetric heating using numerical and analytical approaches.

The novel concept of nanofluids, first introduced by Choi [29] in 1995, has been proposed as a route to surpassing the performance of heat transfer fluids currently available. It is known that heat transfer can be enhanced by employing various techniques and methodologies, such as increasing either the heat transfer surface or the heat transfer coefficient between the fluid and the surface, that allow high heat transfer rates in a small volume [30]. Cooling is one of the most important technical challenges facing many diverse industries, including microelectronics, transportation, solid-state lighting and manufacturing. The addition of micrometer- or millimeter-sized solid metal or metal oxide particles to the base fluids shows an increment in the thermal conductivity of resultant fluids. Nanoparticle materials may be taken as oxide ceramics (Al_2O_3, CuO), metal carbides (SiC), nitrides (AlN, SiN) or metals (Al, Cu), etc. Base fluids are water, ethylene or tri-ethylene–glycols and other coolants, oil and other lubricants, bio-fluids, polymer solutions, other common fluids. In recent years, considerable interest has been evinced in the study of nanofluid and it has become an innovative idea for thermal engineering, because it has various applications in automotive industries, energy saving, nuclear rectors, etc. Further, suspensions of nanoparticles are being developed medical applications including cancer therapy. The solar energy industry has experienced phenomenal growth in recent years due to both technological improvements, resulting in cost reductions, and government policies supportive of renewable energy development and utilization [31]. Owing to their enhanced properties as thermal transfer fluids for instance, nanofluids can be used in a plethora of engineering applications ranging from use in the automotive industry to the medical arena to use in power plant cooling systems as well as computers. Routbort [32] employed nanofluids for industrial cooling that could result in great energy savings and resulting emission reductions. Donzelli et al. [33] showed that a particular class of nanofluids can be used as a smart material working as a heat valve to control the flow of heat. Kim et al. [34] assess the feasibility of nanofluids in nuclear applications by improving the performance of any water-cooled nuclear system that is heat removal limited. Possible applications include pressurized water reactor (PWR) primary coolant, standby safety systems, accelerator targets, plasma diverters. The solar energy industry has experienced phenomenal growth in recent years due to both technological improvements, resulting in cost reductions, and government policies supportive of renewable energy development and utilization. Apart from the application in the field of heat transfer, nanofluids (nanometer particles in a fluid) can also be synthesized for unique magnetic, electrical, chemical and biological applications.

It is worth mentioning that many references on nanofluids can be found in the books by Das et al. [35], Nield and Bejan [36], and Shenoy et al. [37], and in the review papers by Buongiorno [38], Buongiorno et al. [39], Kakaç and Pramuanjaroenkij [40], Lee et al. [41], Fan and Wang [42], Mahian et al. [43], Sheikholeslami and Ganji [44], etc. Buongiorno [38] noted that the nanoparticles absolute velocity can be viewed as the sum of the base fluid velocity and a relative (slip) velocity. He considered in turn seven slip mechanisms: inertia, Brownian diffusion, thermophoresis, diffusiophoresis, Magnus effect, fluid drainage and gravity settling. After examining each of these in turn, he concluded that in the absence of turbulent effects it is the Brownian diffusion and the thermophoresis that will be important. Buongiorno proceeded to write down conservation equations based on these two effects. The thermal instability nanofluid in a porous medium has been also a topic of interest due to its applications in fields of food and chemical process, petroleum industry, bio-mechanics and geophysical problems (see Nield and Kuznetsov [45, 46] and Kuznetsov and Nield [47, 48]). It is worth noting that Sheikholeslami and Chamkha [49] investigated numerically MHD Marangoni boundary layer flow of nanofluid using the Buongiorno model. Some interesting results on nanofluid flow and heat transfer can be found in [50–54].

Here we are dealing with the steady natural convection heat transfer in a cubical enclosure filled with a nanofluid using the mathematical nanofluid model proposed by Buongiorno in combination with the Marangoni convection due to temperature-dependent surface tension at the free surface. To the best of our knowledge, such a problem has not been solved before, so that the present results are new and original.

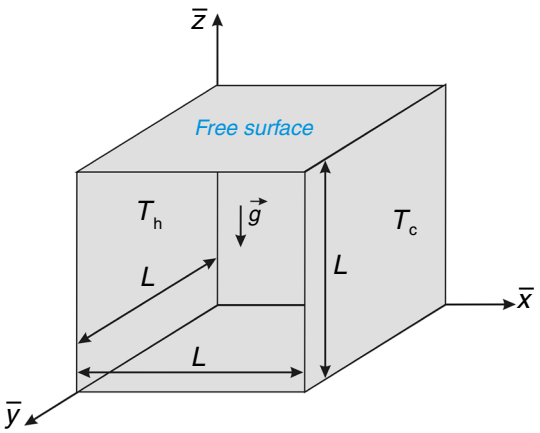

Fig. 1 Physical model and coordinate system

Basic equations

Consider the natural convection heat transfer inside a cubical cavity filled with a water-based nanofluid under the effect of temperature- and concentration-dependent surface tension at the upper free surface. A schematic geometry of the problem under investigation is shown in Fig. 1, where $\bar{x}$, $\bar{y}$ and $\bar{z}$ are the Cartesian coordinates and L is the size of the cavity. It is assumed that the vertical surface $\bar{x} = 0$ is heated and maintained at the constant temperature T_h, while the opposite vertical wall $\bar{x} = L$ is cooled and has the constant temperature T_c. The other walls are adiabatic $(\partial T/\partial \vec{n}) = 0$.

The basic equations for the flow, heat transfer and nanoparticles transport can be written in the following form

$$\nabla \cdot \mathbf{V} = 0 \tag{1}$$

$$\rho_f \left[\frac{\partial \mathbf{V}}{\partial t} + (\mathbf{V}\cdot\nabla)\mathbf{V}\right] = -\nabla p + \mu\nabla^2\mathbf{V} + \left[C\rho_p + (1-C)\rho_{f0}(1-\beta(T-T_c))\right]\mathbf{g} \tag{2}$$

$$\frac{\partial T}{\partial t} + (\mathbf{V}\cdot\nabla T) = \alpha\nabla^2 T + \delta[D_B \nabla C\cdot\nabla T + (D_T/T_c)\nabla T\cdot\nabla T] \tag{3}$$

$$\rho_p\left(\frac{\partial C}{\partial t} + (\mathbf{V}\cdot\nabla C)\right) = -\nabla\cdot\mathbf{j}_p \tag{4}$$

Further on, it is possible to linearize the momentum Eq. (2) in the following form

$$\rho_{f0}\left[\frac{\partial \mathbf{V}}{\partial t} + (\mathbf{V}\cdot\nabla)\mathbf{V}\right] = -\nabla p + \mu\nabla^2\mathbf{V} + \left[C(\rho_p - \rho_{f0}) + \rho_{f0}(1-\beta(T-T_c)(1-C_0))\right]\mathbf{g} \tag{5}$$

Equations (1), (3)–(5) for the problem under consideration can be written in dimensional Cartesian coordinates $\bar{x}$, $\bar{y}$, $\bar{z}$ as

$$\frac{\partial \bar{u}}{\partial \bar{x}} + \frac{\partial \bar{v}}{\partial \bar{y}} + \frac{\partial \bar{w}}{\partial \bar{z}} = 0 \tag{6}$$

$$\rho_{f0}\left[\frac{\partial \bar{u}}{\partial t} + \bar{u}\frac{\partial \bar{u}}{\partial \bar{x}} + \bar{v}\frac{\partial \bar{u}}{\partial \bar{y}} + \bar{w}\frac{\partial \bar{u}}{\partial \bar{z}}\right] = -\frac{\partial p}{\partial \bar{x}} + \mu\left(\frac{\partial^2 \bar{u}}{\partial \bar{x}^2} + \frac{\partial^2 \bar{u}}{\partial \bar{y}^2} + \frac{\partial^2 \bar{u}}{\partial \bar{z}^2}\right) \tag{7}$$

$$\rho_{f0}\left[\frac{\partial \bar{v}}{\partial t} + \bar{u}\frac{\partial \bar{v}}{\partial \bar{x}} + \bar{v}\frac{\partial \bar{v}}{\partial \bar{y}} + \bar{w}\frac{\partial \bar{v}}{\partial \bar{z}}\right] = -\frac{\partial p}{\partial \bar{y}} + \mu\left(\frac{\partial^2 \bar{v}}{\partial \bar{x}^2} + \frac{\partial^2 \bar{v}}{\partial \bar{y}^2} + \frac{\partial^2 \bar{v}}{\partial \bar{z}^2}\right) \tag{8}$$

$$\rho_{f0}\left[\frac{\partial \bar{w}}{\partial t} + \bar{u}\frac{\partial \bar{w}}{\partial \bar{x}} + \bar{v}\frac{\partial \bar{w}}{\partial \bar{y}} + \bar{w}\frac{\partial \bar{w}}{\partial \bar{z}}\right] = -\frac{\partial p}{\partial \bar{z}} + \mu\left(\frac{\partial^2 \bar{w}}{\partial \bar{x}^2} + \frac{\partial^2 \bar{w}}{\partial \bar{y}^2} + \frac{\partial^2 \bar{w}}{\partial \bar{z}^2}\right) - \left[C(\rho_p - \rho_{f0}) + \rho_{f0}(1-\beta(T-T_c)(1-C_0))\right]g \tag{9}$$

$$\frac{\partial T}{\partial t} + \bar{u}\frac{\partial T}{\partial \bar{x}} + \bar{v}\frac{\partial T}{\partial \bar{y}} + \bar{w}\frac{\partial T}{\partial \bar{z}} = \alpha\left(\frac{\partial^2 T}{\partial \bar{x}^2} + \frac{\partial^2 T}{\partial \bar{y}^2} + \frac{\partial^2 T}{\partial \bar{z}^2}\right) + \delta\left\{D_B\left(\frac{\partial C}{\partial \bar{x}}\frac{\partial T}{\partial \bar{x}} + \frac{\partial C}{\partial \bar{y}}\frac{\partial T}{\partial \bar{y}} + \frac{\partial C}{\partial \bar{z}}\frac{\partial T}{\partial \bar{z}}\right) + \left(\frac{D_T}{T_c}\right)\left[\left(\frac{\partial T}{\partial \bar{x}}\right)^2 + \left(\frac{\partial T}{\partial \bar{y}}\right)^2 + \left(\frac{\partial T}{\partial \bar{z}}\right)^2\right]\right\} \tag{10}$$

$$\frac{\partial C}{\partial t} + \bar{u}\frac{\partial C}{\partial \bar{x}} + \bar{v}\frac{\partial C}{\partial \bar{y}} + \bar{w}\frac{\partial C}{\partial \bar{z}} = D_B\left(\frac{\partial^2 C}{\partial \bar{x}^2} + \frac{\partial^2 C}{\partial \bar{y}^2} + \frac{\partial^2 C}{\partial \bar{z}^2}\right) + \left(\frac{D_T}{T_C}\right)\left(\frac{\partial^2 T}{\partial \bar{x}^2} + \frac{\partial^2 T}{\partial \bar{y}^2} + \frac{\partial^2 T}{\partial \bar{z}^2}\right) \tag{11}$$

A transformation of the formulated system of differential Eqs. (6)–(11) to a form eliminating direct search of the pressure field [55–60] is represented as the most reasonable because the aim of the present investigation is the analysis of a thermal state of the system in conditions of natural convection inside the cavity filled with nanofluid. For this purpose, we shall enter into consideration the vector potential functions $\boldsymbol{\psi}$ of the form $\mathbf{V} = \nabla\times\boldsymbol{\psi}$ into the formulation and the vorticity vector $\boldsymbol{\omega}$ of the form $\boldsymbol{\omega} = \nabla\times\mathbf{V}$. It has been shown early (see [55–57]) that the potential is also solenoidal since the velocity is solenoidal (incompressible flow); therefore, $\nabla\cdot\boldsymbol{\psi} = 0$. The velocity components will be defined as follows:

$$\mathbf{V} = \nabla\times\boldsymbol{\psi} \Rightarrow \left\{\bar{u} = \frac{\partial \bar{\psi}_z}{\partial \bar{y}} - \frac{\partial \bar{\psi}_y}{\partial \bar{z}},\ \bar{v} = \frac{\partial \bar{\psi}_x}{\partial \bar{z}} - \frac{\partial \bar{\psi}_z}{\partial \bar{x}},\ \bar{w} = \frac{\partial \bar{\psi}_y}{\partial \bar{x}} - \frac{\partial \bar{\psi}_x}{\partial \bar{y}}\right\} \tag{12}$$

and the vorticity components can be defined as follows:

$$\boldsymbol{\omega} = \nabla\times\mathbf{V} \Rightarrow \left\{\bar{\omega}_x = \frac{\partial \bar{w}}{\partial \bar{y}} - \frac{\partial \bar{v}}{\partial \bar{z}},\ \bar{\omega}_y = \frac{\partial \bar{u}}{\partial \bar{z}} - \frac{\partial \bar{w}}{\partial \bar{x}},\ \bar{\omega}_z = \frac{\partial \bar{v}}{\partial \bar{x}} - \frac{\partial \bar{u}}{\partial \bar{y}}\right\} \tag{13}$$

so that Eq. (6) is satisfied identically. We are then left with the following equations taking into account the steady-state regime

$$\frac{\partial^2\bar{\psi}_x}{\partial\bar{x}^2}+\frac{\partial^2\bar{\psi}_x}{\partial\bar{y}^2}+\frac{\partial^2\bar{\psi}_x}{\partial\bar{z}^2}=-\bar{\omega}_x \tag{14}$$

$$\frac{\partial^2\bar{\psi}_y}{\partial\bar{x}^2}+\frac{\partial^2\bar{\psi}_y}{\partial\bar{y}^2}+\frac{\partial^2\bar{\psi}_y}{\partial\bar{z}^2}=-\bar{\omega}_y \tag{15}$$

$$\frac{\partial^2\bar{\psi}_z}{\partial\bar{x}^2}+\frac{\partial^2\bar{\psi}_z}{\partial\bar{y}^2}+\frac{\partial^2\bar{\psi}_z}{\partial\bar{z}^2}=-\bar{\omega}_z \tag{16}$$

$$\begin{aligned}
&\rho_{f0}\left[\left(\frac{\partial\bar{\psi}_z}{\partial\bar{y}}-\frac{\partial\bar{\psi}_y}{\partial\bar{z}}\right)\frac{\partial\bar{\omega}_x}{\partial\bar{x}}+\left(\frac{\partial\bar{\psi}_x}{\partial\bar{z}}-\frac{\partial\bar{\psi}_z}{\partial\bar{x}}\right)\frac{\partial\bar{\omega}_x}{\partial\bar{y}}\right.\\
&\quad+\left(\frac{\partial\bar{\psi}_y}{\partial\bar{x}}-\frac{\partial\bar{\psi}_x}{\partial\bar{y}}\right)\frac{\partial\bar{\omega}_x}{\partial\bar{z}}-\bar{\omega}_x\frac{\partial}{\partial\bar{x}}\left(\frac{\partial\bar{\psi}_z}{\partial\bar{y}}-\frac{\partial\bar{\psi}_y}{\partial\bar{z}}\right)\\
&\quad\left.-\bar{\omega}_y\frac{\partial}{\partial\bar{y}}\left(\frac{\partial\bar{\psi}_z}{\partial\bar{y}}-\frac{\partial\bar{\psi}_y}{\partial\bar{z}}\right)-\bar{\omega}_z\frac{\partial}{\partial\bar{z}}\left(\frac{\partial\bar{\psi}_z}{\partial\bar{y}}-\frac{\partial\bar{\psi}_y}{\partial\bar{z}}\right)\right]\\
&=\mu\left(\frac{\partial^2\bar{\omega}_x}{\partial\bar{x}^2}+\frac{\partial^2\bar{\omega}_x}{\partial\bar{y}^2}+\frac{\partial^2\bar{\omega}_x}{\partial\bar{z}^2}\right)\\
&\quad+\rho_{f0}\beta(1-C_0)g\frac{\partial T}{\partial\bar{y}}-g\left(\rho_p-\rho_{f0}\right)\frac{\partial C}{\partial\bar{y}}
\end{aligned} \tag{17}$$

$$\begin{aligned}
&\rho_{f0}\left[\left(\frac{\partial\bar{\psi}_z}{\partial\bar{y}}-\frac{\partial\bar{\psi}_y}{\partial\bar{z}}\right)\frac{\partial\bar{\omega}_y}{\partial\bar{x}}+\left(\frac{\partial\bar{\psi}_x}{\partial\bar{z}}-\frac{\partial\bar{\psi}_z}{\partial\bar{x}}\right)\frac{\partial\bar{\omega}_y}{\partial\bar{y}}\right.\\
&\quad+\left(\frac{\partial\bar{\psi}_y}{\partial\bar{x}}-\frac{\partial\bar{\psi}_x}{\partial\bar{y}}\right)\frac{\partial\bar{\omega}_y}{\partial\bar{z}}-\bar{\omega}_x\frac{\partial}{\partial\bar{x}}\left(\frac{\partial\bar{\psi}_x}{\partial\bar{z}}-\frac{\partial\bar{\psi}_z}{\partial\bar{x}}\right)\\
&\quad\left.-\bar{\omega}_y\frac{\partial}{\partial\bar{y}}\left(\frac{\partial\bar{\psi}_x}{\partial\bar{z}}-\frac{\partial\bar{\psi}_z}{\partial\bar{x}}\right)-\bar{\omega}_z\frac{\partial}{\partial\bar{z}}\left(\frac{\partial\bar{\psi}_x}{\partial\bar{z}}-\frac{\partial\bar{\psi}_z}{\partial\bar{x}}\right)\right]\\
&=\mu\left(\frac{\partial^2\bar{\omega}_y}{\partial\bar{x}^2}+\frac{\partial^2\bar{\omega}_y}{\partial\bar{y}^2}+\frac{\partial^2\bar{\omega}_y}{\partial\bar{z}^2}\right)\\
&\quad-\rho_{f0}\beta(1-C_0)g\frac{\partial T}{\partial\bar{x}}+g\left(\rho_p-\rho_{f0}\right)\frac{\partial C}{\partial\bar{x}}
\end{aligned} \tag{18}$$

$$\begin{aligned}
&\rho_{f0}\left[\left(\frac{\partial\bar{\psi}_z}{\partial\bar{y}}-\frac{\partial\bar{\psi}_y}{\partial\bar{z}}\right)\frac{\partial\bar{\omega}_z}{\partial\bar{x}}+\left(\frac{\partial\bar{\psi}_x}{\partial\bar{z}}-\frac{\partial\bar{\psi}_z}{\partial\bar{x}}\right)\frac{\partial\bar{\omega}_z}{\partial\bar{y}}\right.\\
&\quad+\left(\frac{\partial\bar{\psi}_y}{\partial\bar{x}}-\frac{\partial\bar{\psi}_x}{\partial\bar{y}}\right)\frac{\partial\bar{\omega}_z}{\partial\bar{z}}-\bar{\omega}_x\frac{\partial}{\partial\bar{x}}\left(\frac{\partial\bar{\psi}_y}{\partial\bar{x}}-\frac{\partial\bar{\psi}_x}{\partial\bar{y}}\right)\\
&\quad\left.-\bar{\omega}_y\frac{\partial}{\partial\bar{y}}\left(\frac{\partial\bar{\psi}_y}{\partial\bar{x}}-\frac{\partial\bar{\psi}_x}{\partial\bar{y}}\right)-\bar{\omega}_z\frac{\partial}{\partial\bar{z}}\left(\frac{\partial\bar{\psi}_y}{\partial\bar{x}}-\frac{\partial\bar{\psi}_x}{\partial\bar{y}}\right)\right]\\
&=\mu\left(\frac{\partial^2\bar{\omega}_z}{\partial\bar{x}^2}+\frac{\partial^2\bar{\omega}_z}{\partial\bar{y}^2}+\frac{\partial^2\bar{\omega}_z}{\partial\bar{z}^2}\right)
\end{aligned} \tag{19}$$

$$\begin{aligned}
&\left(\frac{\partial\bar{\psi}_z}{\partial\bar{y}}-\frac{\partial\bar{\psi}_y}{\partial\bar{z}}\right)\frac{\partial T}{\partial\bar{x}}+\left(\frac{\partial\bar{\psi}_x}{\partial\bar{z}}-\frac{\partial\bar{\psi}_z}{\partial\bar{x}}\right)\frac{\partial T}{\partial\bar{y}}\\
&\quad+\left(\frac{\partial\bar{\psi}_y}{\partial\bar{x}}-\frac{\partial\bar{\psi}_x}{\partial\bar{y}}\right)\frac{\partial T}{\partial\bar{z}}=\alpha\left(\frac{\partial^2T}{\partial\bar{x}^2}+\frac{\partial^2T}{\partial\bar{y}^2}+\frac{\partial^2T}{\partial\bar{z}^2}\right)\\
&\quad+\delta\left\{D_B\left(\frac{\partial C}{\partial\bar{x}}\frac{\partial T}{\partial\bar{x}}+\frac{\partial C}{\partial\bar{y}}\frac{\partial T}{\partial\bar{y}}+\frac{\partial C}{\partial\bar{z}}\frac{\partial T}{\partial\bar{z}}\right)\right.\\
&\quad\left.+\left(\frac{D_T}{T_c}\right)\left[\left(\frac{\partial T}{\partial\bar{x}}\right)^2+\left(\frac{\partial T}{\partial\bar{y}}\right)^2+\left(\frac{\partial T}{\partial\bar{z}}\right)^2\right]\right\}
\end{aligned} \tag{20}$$

$$\begin{aligned}
&\left(\frac{\partial\bar{\psi}_z}{\partial\bar{y}}-\frac{\partial\bar{\psi}_y}{\partial\bar{z}}\right)\frac{\partial C}{\partial\bar{x}}+\left(\frac{\partial\bar{\psi}_x}{\partial\bar{z}}-\frac{\partial\bar{\psi}_z}{\partial\bar{x}}\right)\frac{\partial C}{\partial\bar{y}}\\
&\quad+\left(\frac{\partial\bar{\psi}_y}{\partial\bar{x}}-\frac{\partial\bar{\psi}_x}{\partial\bar{y}}\right)\frac{\partial C}{\partial\bar{z}}\\
&=D_B\left(\frac{\partial^2C}{\partial\bar{x}^2}+\frac{\partial^2C}{\partial\bar{y}^2}+\frac{\partial^2C}{\partial\bar{z}^2}\right)\\
&\quad+\left(\frac{D_T}{T_C}\right)\left(\frac{\partial^2T}{\partial\bar{x}^2}+\frac{\partial^2T}{\partial\bar{y}^2}+\frac{\partial^2T}{\partial\bar{z}^2}\right)
\end{aligned} \tag{21}$$

Introducing the following dimensionless variables

$$\begin{aligned}
&x=\bar{x}/L,\quad y=\bar{y}/L,\quad z=\bar{z}/L,\\
&\psi_x=\bar{\psi}_x\Big/\sqrt{(1-C_0)g\rho_{f0}\beta\Delta TL^3},\\
&\psi_y=\bar{\psi}_y\Big/\sqrt{(1-C_0)g\rho_{f0}\beta\Delta TL^3},\\
&\psi_z=\bar{\psi}_z\Big/\sqrt{(1-C_0)g\rho_{f0}\beta\Delta TL^3},\\
&\omega_x=\bar{\omega}_x\sqrt{(1-C_0)g\rho_{f0}\beta\Delta T/L},\\
&\omega_y=\bar{\omega}_y\sqrt{(1-C_0)g\rho_{f0}\beta\Delta T/L},\\
&\omega_z=\bar{\omega}_z\sqrt{(1-C_0)g\rho_{f0}\beta\Delta T/L},\\
&\theta=(T-T_0)/(T_h-T_c),\quad \phi=C/C_0
\end{aligned} \tag{22}$$

where $T_0=(T_h+T_c)/2$ is the mean temperature of heated and cooled walls, and substituting (22) into Eqs. (14)–(21), we obtain

$$\frac{\partial^2\psi_x}{\partial x^2}+\frac{\partial^2\psi_x}{\partial y^2}+\frac{\partial^2\psi_x}{\partial z^2}=-\omega_x \tag{23}$$

$$\frac{\partial^2\psi_y}{\partial x^2}+\frac{\partial^2\psi_y}{\partial y^2}+\frac{\partial^2\psi_y}{\partial z^2}=-\omega_y \tag{24}$$

$$\frac{\partial^2\psi_z}{\partial x^2}+\frac{\partial^2\psi_z}{\partial y^2}+\frac{\partial^2\psi_z}{\partial z^2}=-\omega_z \tag{25}$$

$$\left(\frac{\partial\psi_z}{\partial y}-\frac{\partial\psi_y}{\partial z}\right)\frac{\partial\omega_x}{\partial x}+\left(\frac{\partial\psi_x}{\partial z}-\frac{\partial\psi_z}{\partial x}\right)\frac{\partial\omega_x}{\partial y}+\left(\frac{\partial\psi_y}{\partial x}-\frac{\partial\psi_x}{\partial y}\right)\frac{\partial\omega_x}{\partial z}-\omega_x\frac{\partial}{\partial x}\left(\frac{\partial\psi_z}{\partial y}-\frac{\partial\psi_y}{\partial z}\right)-\omega_y\frac{\partial}{\partial y}\left(\frac{\partial\psi_z}{\partial y}-\frac{\partial\psi_y}{\partial z}\right)-\omega_z\frac{\partial}{\partial z}\left(\frac{\partial\psi_z}{\partial y}-\frac{\partial\psi_y}{\partial z}\right)=\sqrt{\frac{\mathrm{Pr}}{Ra}}\left(\frac{\partial^2\omega_x}{\partial x^2}+\frac{\partial^2\omega_x}{\partial y^2}+\frac{\partial^2\omega_x}{\partial z^2}\right)+\frac{\partial\theta}{\partial y}-Nr\frac{\partial\phi}{\partial y} \tag{26}$$

$$\left(\frac{\partial\psi_z}{\partial y}-\frac{\partial\psi_y}{\partial z}\right)\frac{\partial\omega_y}{\partial x}+\left(\frac{\partial\psi_x}{\partial z}-\frac{\partial\psi_z}{\partial x}\right)\frac{\partial\omega_y}{\partial y}+\left(\frac{\partial\psi_y}{\partial x}-\frac{\partial\psi_x}{\partial y}\right)\frac{\partial\omega_y}{\partial z}-\omega_x\frac{\partial}{\partial x}\left(\frac{\partial\psi_x}{\partial z}-\frac{\partial\psi_z}{\partial x}\right)-\omega_y\frac{\partial}{\partial y}\left(\frac{\partial\psi_x}{\partial z}-\frac{\partial\psi_z}{\partial x}\right)-\omega_z\frac{\partial}{\partial z}\left(\frac{\partial\psi_x}{\partial z}-\frac{\partial\psi_z}{\partial x}\right)=\sqrt{\frac{\mathrm{Pr}}{Ra}}\left(\frac{\partial^2\omega_y}{\partial x^2}+\frac{\partial^2\omega_y}{\partial y^2}+\frac{\partial^2\omega_y}{\partial z^2}\right)-\frac{\partial\theta}{\partial x}+Nr\frac{\partial\phi}{\partial x} \tag{27}$$

$$\left(\frac{\partial\psi_z}{\partial y}-\frac{\partial\psi_y}{\partial z}\right)\frac{\partial\omega_z}{\partial x}+\left(\frac{\partial\psi_x}{\partial z}-\frac{\partial\psi_z}{\partial x}\right)\frac{\partial\omega_z}{\partial y}+\left(\frac{\partial\psi_y}{\partial x}-\frac{\partial\psi_x}{\partial y}\right)\frac{\partial\omega_z}{\partial z}-\omega_x\frac{\partial}{\partial x}\left(\frac{\partial\psi_y}{\partial x}-\frac{\partial\psi_x}{\partial y}\right)-\omega_y\frac{\partial}{\partial y}\left(\frac{\partial\psi_y}{\partial x}-\frac{\partial\psi_x}{\partial y}\right)-\omega_z\frac{\partial}{\partial z}\left(\frac{\partial\psi_y}{\partial x}-\frac{\partial\psi_x}{\partial y}\right)=\sqrt{\frac{\mathrm{Pr}}{Ra}}\left(\frac{\partial^2\omega_z}{\partial x^2}+\frac{\partial^2\omega_z}{\partial y^2}+\frac{\partial^2\omega_z}{\partial z^2}\right) \tag{28}$$

$$\left(\frac{\partial\psi_z}{\partial y}-\frac{\partial\psi_y}{\partial z}\right)\frac{\partial\theta}{\partial x}+\left(\frac{\partial\psi_x}{\partial z}-\frac{\partial\psi_z}{\partial x}\right)\frac{\partial\theta}{\partial y}+\left(\frac{\partial\psi_y}{\partial x}-\frac{\partial\psi_x}{\partial y}\right)\frac{\partial\theta}{\partial z}=\frac{1}{\sqrt{Ra\cdot\mathrm{Pr}}}\left(\frac{\partial^2\theta}{\partial x^2}+\frac{\partial^2\theta}{\partial y^2}+\frac{\partial^2\theta}{\partial z^2}\right)+\frac{Nb}{\sqrt{Ra\cdot\mathrm{Pr}}}\left(\frac{\partial\phi}{\partial x}\frac{\partial\theta}{\partial x}+\frac{\partial\phi}{\partial y}\frac{\partial\theta}{\partial y}+\frac{\partial\phi}{\partial z}\frac{\partial\theta}{\partial z}\right)+\frac{Nt}{\sqrt{Ra\cdot\mathrm{Pr}}}\left[\left(\frac{\partial\theta}{\partial x}\right)^2+\left(\frac{\partial\theta}{\partial y}\right)^2+\left(\frac{\partial\theta}{\partial z}\right)^2\right]\Bigg\} \tag{29}$$

$$\left(\frac{\partial\psi_z}{\partial y}-\frac{\partial\psi_y}{\partial z}\right)\frac{\partial\phi}{\partial x}+\left(\frac{\partial\psi_x}{\partial z}-\frac{\partial\psi_z}{\partial x}\right)\frac{\partial\phi}{\partial y}+\left(\frac{\partial\psi_y}{\partial x}-\frac{\partial\psi_x}{\partial y}\right)\frac{\partial\phi}{\partial z}=\frac{1}{Le\sqrt{Ra\cdot\mathrm{Pr}}}\left(\frac{\partial^2\phi}{\partial x^2}+\frac{\partial^2\phi}{\partial y^2}+\frac{\partial^2\phi}{\partial z^2}\right)+\frac{1}{Le\sqrt{Ra\cdot\mathrm{Pr}}}\frac{Nt}{Nb}\left(\frac{\partial^2\theta}{\partial x^2}+\frac{\partial^2\theta}{\partial y^2}+\frac{\partial^2\theta}{\partial z^2}\right) \tag{30}$$

The corresponding boundary conditions for these equations are given by

$$\frac{\partial\psi_x}{\partial x}=\psi_y=\psi_z=0,\omega_x=0,\omega_y=-\frac{\partial^2\psi_y}{\partial x^2},$$
$$\omega_z=-\frac{\partial^2\psi_z}{\partial x^2},\theta=0.5,Nb\frac{\partial\phi}{\partial x}+Nt\frac{\partial\theta}{\partial x}=0\text{ on }x=0$$
$$\frac{\partial\psi_x}{\partial x}=\psi_y=\psi_z=0,\omega_x=0,\omega_y=-\frac{\partial^2\psi_y}{\partial x^2},$$
$$\omega_z=-\frac{\partial^2\psi_z}{\partial x^2},\theta=-0.5,Nb\frac{\partial\phi}{\partial x}+Nt\frac{\partial\theta}{\partial x}=0\text{ on }x=1$$
$$\psi_x=\frac{\partial\psi_y}{\partial y}=\psi_z=0,\omega_x=-\frac{\partial^2\psi_x}{\partial y^2},$$
$$\omega_y=0,\omega_z=-\frac{\partial^2\psi_z}{\partial y^2},\frac{\partial\theta}{\partial y}=0,\frac{\partial\phi}{\partial y}=0\text{ on}$$
$$y=0\text{ and }y=1$$
$$\psi_x=\psi_y=\frac{\partial\psi_z}{\partial z}=0,\omega_x=-\frac{\partial^2\psi_x}{\partial z^2},\omega_y=-\frac{\partial^2\psi_y}{\partial z^2},$$
$$\omega_z=0,\frac{\partial\theta}{\partial z}=0,\frac{\partial\phi}{\partial z}=0\text{ on }z=0$$
$$\psi_x=\psi_y=\frac{\partial\psi_z}{\partial z}=0,\frac{\partial\theta}{\partial z}=0,\frac{\partial\phi}{\partial z}=0\text{ on }z=1 \tag{31}$$

where key parameters are defined as

$$Ra=\frac{(1-C_0)g\rho_{f0}\beta\Delta TL}{\alpha\mu},\quad Nr=\frac{(\rho_p-\rho_{f0})C_0}{\rho_{f0}\beta\Delta T(1-C_0)},$$
$$Nb=\frac{\delta D_B C_0}{\alpha},\quad Nt=\frac{\delta D_T\Delta T}{\alpha T_c},\quad Le=\frac{\alpha}{D_B} \tag{32}$$

It should be noted that at free surface we have the following conditions:

$$\begin{cases}\mu\dfrac{\partial\bar{u}}{\partial\bar{z}}\Big|_{\bar{z}=L}=-\left(\dfrac{\partial\sigma}{\partial T}\dfrac{\partial T}{\partial\bar{x}}\Big|_{\bar{z}=L}+\dfrac{\partial\sigma}{\partial C}\dfrac{\partial C}{\partial\bar{x}}\Big|_{\bar{z}=L}\right)\\ \mu\dfrac{\partial\bar{v}}{\partial\bar{z}}\Big|_{\bar{z}=L}=-\left(\dfrac{\partial\sigma}{\partial T}\dfrac{\partial T}{\partial\bar{y}}\Big|_{\bar{z}=L}+\dfrac{\partial\sigma}{\partial C}\dfrac{\partial C}{\partial\bar{y}}\Big|_{\bar{z}=L}\right)\end{cases} \tag{33}$$

Taking into account dimensionless variables (22), Eqs. (33) can be written as:

$$\begin{cases}\dfrac{\partial u}{\partial z}\Big|_{z=1}=\dfrac{Ma_T}{\sqrt{Ra\cdot\mathrm{Pr}}}\dfrac{\partial\theta}{\partial x}\Big|_{z=1}+\dfrac{Ma_C}{Le\sqrt{Ra\cdot\mathrm{Pr}}}\dfrac{\partial\phi}{\partial x}\Big|_{z=1}\\ \dfrac{\partial v}{\partial z}\Big|_{z=1}=\dfrac{Ma_T}{\sqrt{Ra\cdot\mathrm{Pr}}}\dfrac{\partial\theta}{\partial y}\Big|_{z=1}+\dfrac{Ma_C}{Le\sqrt{Ra\cdot\mathrm{Pr}}}\dfrac{\partial\phi}{\partial y}\Big|_{z=1}\end{cases} \tag{34}$$

Further, we can use a definition of vorticity components in dimensionless form and for the free surface where $w=0$, we have:

$$\omega_x|_{z=1} = -\left.\frac{\partial v}{\partial z}\right|_{z=1} = -\frac{Ma_T}{\sqrt{Ra\cdot \mathrm{Pr}}}\left.\frac{\partial \theta}{\partial y}\right|_{z=1} - \frac{Ma_C}{Le\sqrt{Ra\cdot \mathrm{Pr}}}\left.\frac{\partial \phi}{\partial y}\right|_{z=1}$$
$$\omega_y|_{z=1} = \left.\frac{\partial u}{\partial z}\right|_{z=1} = \frac{Ma_T}{\sqrt{Ra\cdot \mathrm{Pr}}}\left.\frac{\partial \theta}{\partial x}\right|_{z=1} + \frac{Ma_C}{Le\sqrt{Ra\cdot \mathrm{Pr}}}\left.\frac{\partial \phi}{\partial x}\right|_{z=1}$$
$$\omega_z|_{z=1} = 0 \tag{35}$$

As regards boundary condition (31), it is worth pointing out that Nield and Kuznetsov [45] have assumed that one could control the value of the nanoparticle fraction at the boundary in the same way as the temperature there could be controlled, but no indication was given of how this could be done in practice. Thus, in the recently published papers by Nield and Kuznetsov [45] and Kuznetsov and Nield [48], they have replaced the boundary conditions by a set that are more realistic physically, assuming that there is no nanoparticle flux at the plate and that the particle fraction value there adjusts accordingly.

The physical quantities of interest are the local Nusselt (Nu) and Sherwood (Sh) numbers, which are defined as

$$Nu = -(\partial\theta/\partial x)_{x=0}, \quad Sh = -(\partial\phi/\partial x)_{x=0} \tag{36}$$

and the average Nusselt ($\overline{Nu}$) and Sherwood ($\overline{Sh}$) numbers, which are given by

$$\overline{Nu} = \int_0^1\int_0^1 Nu\,\mathrm{d}y\mathrm{d}z, \quad \overline{Sh} = \int_0^1\int_0^1 Sh\,\mathrm{d}y\mathrm{d}z \tag{37}$$

It is worth noting that for an analysis of the Sherwood number along the heated wall it is possible to study only Nusselt number along this wall because at this wall we have $\partial\phi/\partial x = -Nt/Nb(\partial\theta/\partial x)$ taking into account boundary conditions for ϕ [Eqs. (31)]. Therefore, the further analysis concerning integral parameters will be conducted only for the average Nusselt number because $Sh = -(Nt/Nb)Nu$ and $\overline{Sh} = -(Nt/Nb)\overline{Nu}$.

Numerical method

Partial differential Eqs. (23)–(30) with corresponding boundary conditions (31) are solved by the finite difference method. Detailed description of the used numerical technique is presented in [37, 55–57]. The present models, in the form of an in-house computational fluid dynamics (CFD) code, have been validated successfully (see [55–57]).

For the purpose of obtaining grid-independent solution, a grid sensitivity analysis is performed. The grid-independent solution was performed by preparing the solution for free convection in a cubical cavity filled with a water-based nanofluid at $Ra = 10^5$, $Pr = 7.0$, $Le = 100$, $Nr = 0.1$, $Nb = 0.1$, $Nt = 0.1$, $Ma_T = Ma_C = 1000$. Four cases of uniform grid are tested: a grid of $30 \times 30 \times 30$ points, a grid of $50 \times 50 \times 50$ points, a grid of $70 \times 70 \times 70$ points and a much finer grid of $100 \times 100 \times 100$ points. Table 1 shows an effect of the mesh parameters on the average Nusselt number of the hot wall.

On the basis of the conducted verifications, the uniform mesh of $50 \times 50 \times 50$ points has been selected for the following analysis.

Table 1 Variations of the average Nusselt number of the heat wall

Uniform grids	$\overline{Nu}$	$\Delta = \frac{\lvert\overline{Nu}_{i\times j} - \overline{Nu}_{50\times 50\times 50}\rvert}{\overline{Nu}_{i\times j}} \times 100\%$
$30 \times 30 \times 30$	4.869	9.08
$50 \times 50 \times 50$	4.427	–
$70 \times 70 \times 70$	4.343	1.93
$100 \times 100 \times 100$	4.312	2.67

Results and discussion

Numerical investigation of boundary value problem (23)–(31) has been carried out at the following values of key parameters: Rayleigh number ($Ra = 10^5$), Lewis number ($Le = 10$–1000), Marangoni number ($Ma_T = Ma_C = Ma = 10$–1000), the buoyancy ratio parameter ($Nr = 0.1$–0.5), the Brownian motion parameter ($Nb = 0.1$–0.5) and the thermophoresis parameter ($Nt = 0.1$–0.5). Particular efforts have been focused on the effects of these key parameters on the fluid flow, heat and mass transfer characteristics.

Figure 2 shows three-dimensional velocity, temperature and nanoparticle concentration fields for $Le = 1000$, $Nr = 0.1$, $Nt = 0.1$, $Nb = 0.1$ and different values of the Marangoni number. It should be noted that low values of the Marangoni numbers do not have any effect on nanofluid flow and heat transfer inside the cavity. Therefore, one can find a formation of an ascending flow near the hot wall $x = 0$ and descending flow close to the cold wall $x = 1$. At the same time, the flow patterns in central part of the cube are complicated illustrating an appearance of internal helical flows from the center to the adiabatic walls $y = 0$ and $y = 1$. This motion is very interesting and complex. It is possible to observe a global circulation from hot wall to cold one and a complex one from central part of the cavity where we have convective cell cores to adiabatic wall within the helix of small radius. Moving away from the central part, a radius of the helical flow rates up to the adiabatic wall. After approaching the adiabatic walls $y = 0$ and $y = 1$, this helical flow reverses to the central part also increasing the helical flow radius. Such process continues up to penetration into the global circulation. It is worth

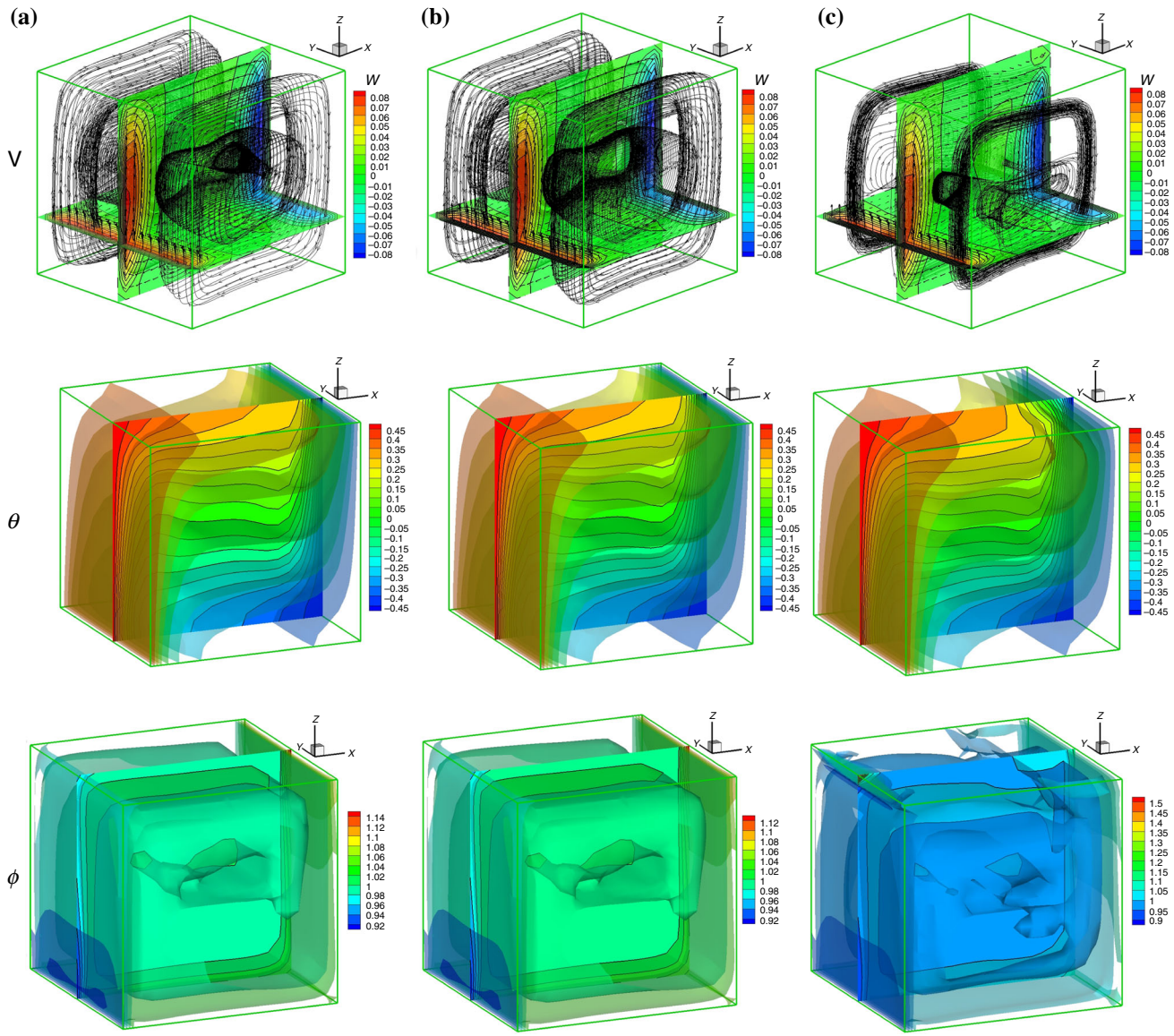

Fig. 2 Three-dimensional velocity V, temperature θ and nanoparticles volume fraction ϕ fields for $Le = 1000$, $Nr = 0.1$, $Nt = 0.1$, $Nb = 0.1$: $Ma = 10$ (**a**), $Ma = 100$ (**b**), $Ma = 1000$ (**c**)

noting a formation of ascending thermal boundary layer along the wall $x = 0$ and descending thermal boundary layer near the cold wall $x = 1$, while the central part has a thermally stratification core where heat transfers from the upper part to the bottom one by heat conduction. Nanoparticles volume fraction reflects a diminution of nanoparticles concentration at the bottom part of the hoot wall and a growth of the nanoparticles volume fraction near the upper part of the cold wall. Such behavior can be explained by the thermophoresis effect when nanoparticles transport occurs along the heat flux from the hot wall to the cold one. At the same time, concentration of nanoparticles in the cavity central part does not change.

The Marangoni number characterizes an effect of the surface tension rate with temperature and concentration. Therefore, for high value of Ma (1000) one can find a growth of the shear stress at free surface and as a result we have a formation of additional circulation near the upper right corner ($x \approx 1$ and $z \approx 1$). Mentioned modification results in the temperature reduction in this zone.

More pictorial distributions of the velocity, temperature and nanoparticles concentration are presented in Fig. 3 for the middle cross section $y = 0.5$. For $Ma = 10$ and 100 (Fig. 3a, b) flow patterns, temperature and concentration fields have insignificant changes. At the same time, an appearance of different convective cell cores is due to the origin of recirculation flow in the upper right corner. As has

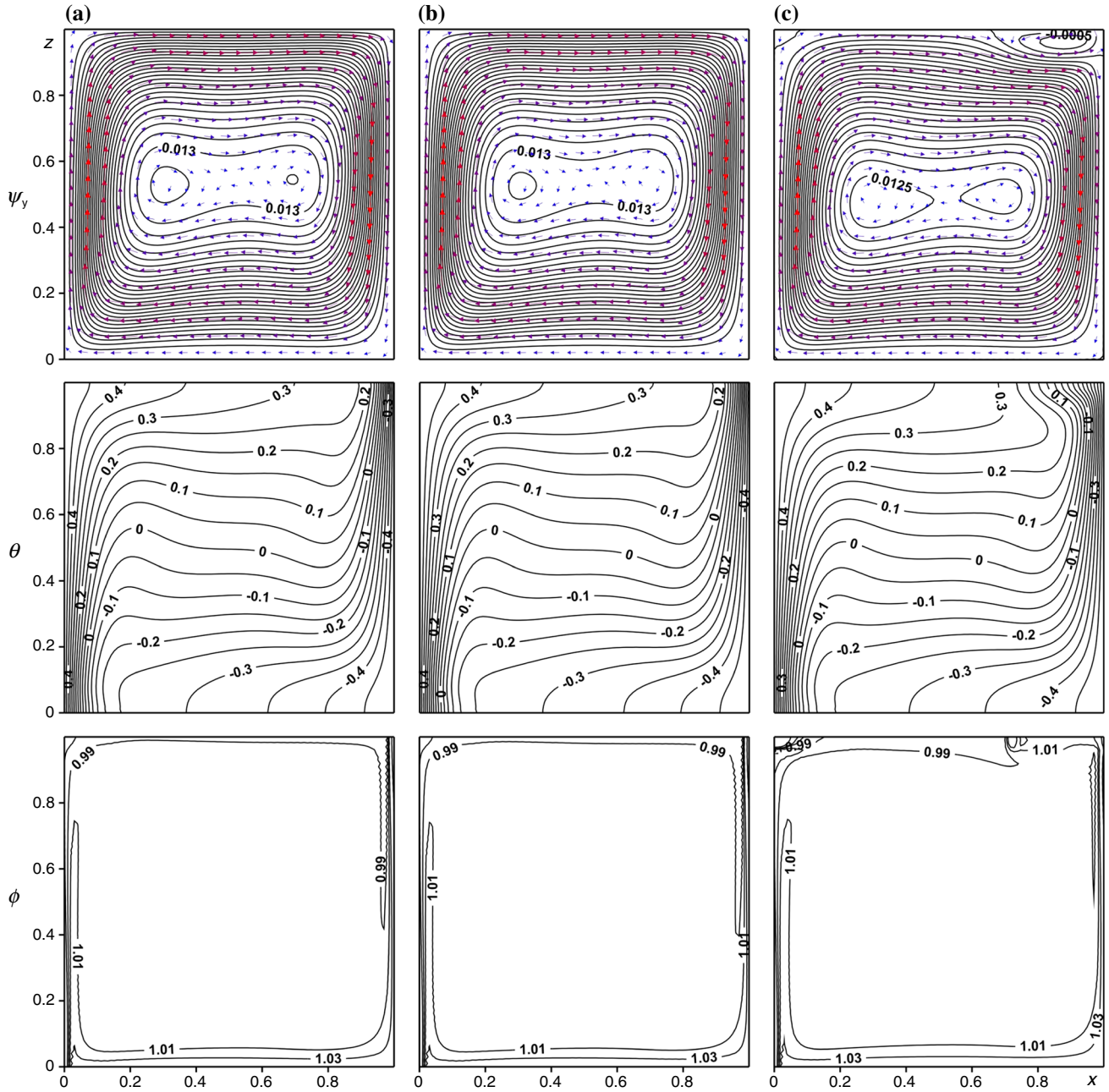

Fig. 3 Streamlines ψ_y, isotherms θ and nanoparticles volume fraction ϕ for $Le = 1000$, $Nr = 0.1$, $Nt = 0.1$, $Nb = 0.1$: $Ma = 10$ (**a**), $Ma = 100$ (**b**), $Ma = 1000$ (**c**)

been mentioned above, for $Ma = 1000$ (Fig. 3c) one can find a formation of a circulation in the upper right corner owing to an increasing surface tension that in dependence on the temperature and nanoparticles concentration. At the same time, small vortex can be found also in the upper left corner. Further growth of the Marangoni number can lead to an extension of this recirculation. At the same time, this minor recirculation changes the temperature field in the upper right corner where more essential cooling occurs. As a result, nanoparticles concentration also increases in this part due to a formation of a recirculation as a stagnation zone.

Figure 4 illustrates the effect of the Lewis number on velocity field, isotherms and nanoparticle isoconcentrations in the middle cross section of the cavity $y = 0.5$ for $Ma = 1000$, $Nr = 0.1$, $Nt = 0.1$, $Nb = 0.1$. A growth of the Lewis number leads to a weak intensification of the major convective flow, while the temperature field does not change. Main modification can be found in distributions of isoconcentration lines due to a reduction of the

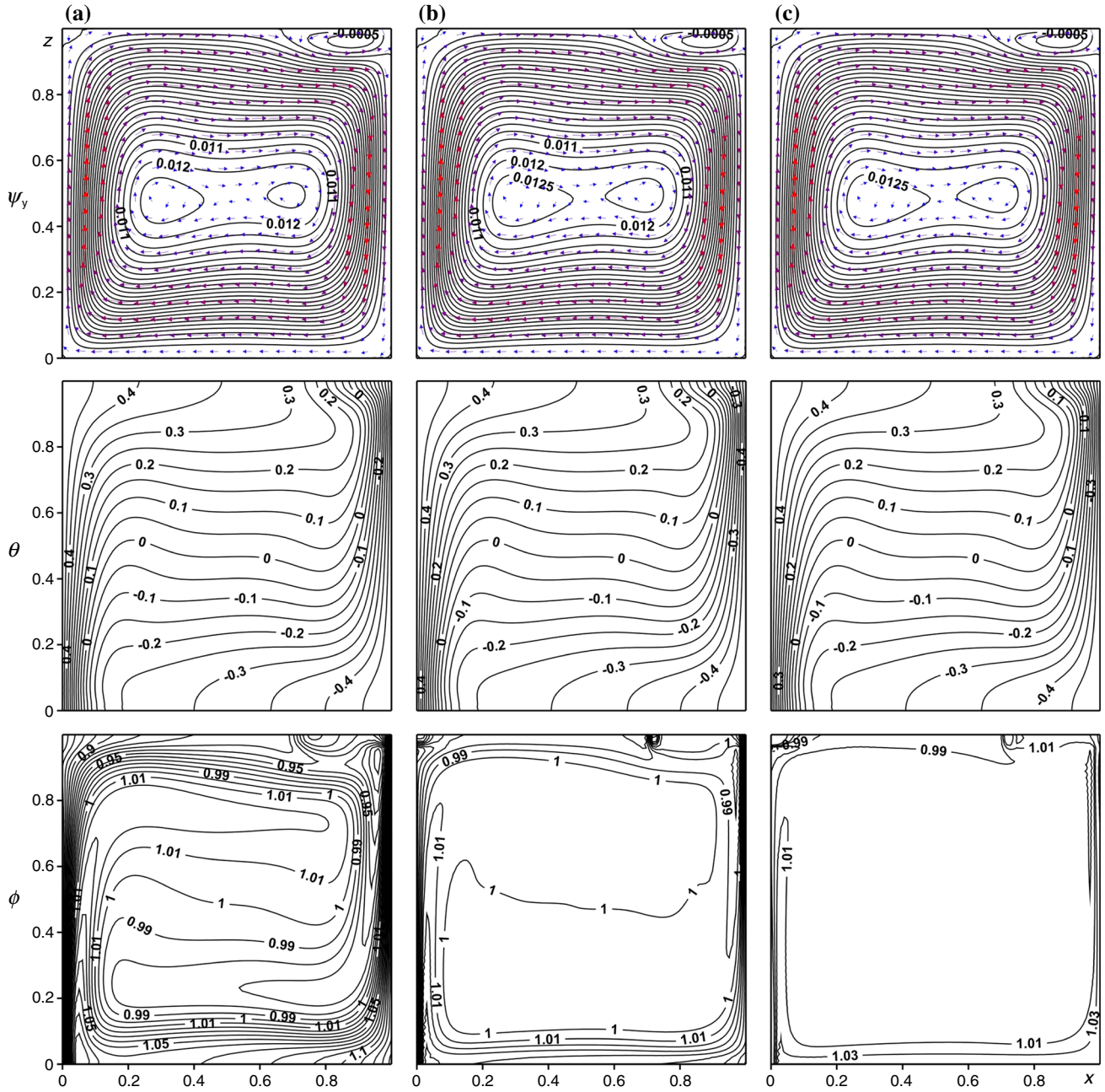

Fig. 4 Streamlines ψ_y, isotherms θ and nanoparticles volume fraction ϕ for $Ma = 1000$, $Nr = 0.1$, $Nt = 0.1$, $Nb = 0.1$: $Le = 10$ (**a**), $Le = 100$ (**b**), $Le = 1000$ (**c**)

concentration boundary layer thickness with a growth of the Lewis number. Moreover, high values of *Le* characterize more homogeneous distribution of nanoparticles inside the cubical cavity.

The effects of the governing parameters on the heat transfer rate are presented in Figs. 5 and 6. A growth of the Lewis number, Marangoni number and thermophoresis parameter results in the heat transfer rate reduction. More essential influence of the Lewis number occurs for the transition between $Le = 10$ and $Le = 100$, while the average Nusselt number changes insignificantly with the Brownian diffusion parameter and buoyancy ratio parameter for the considered range of these coefficients. It should be noted that the thermophoresis effect is more essential in comparison with Brownian diffusion and buoyancy effect. It seems that the main reason for such behavior is the significant influence of heat flux from the heated wall in the case of thin concentration boundary layer.

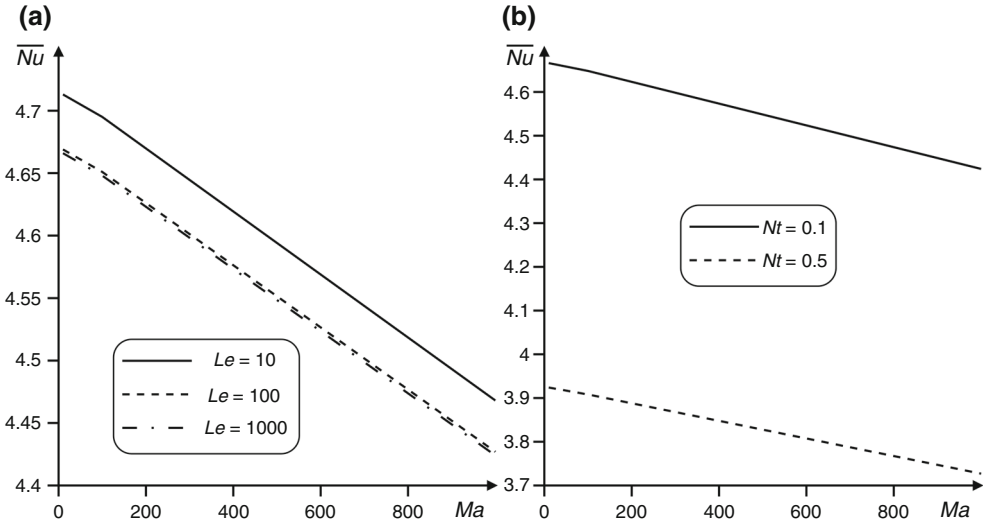

Fig. 5 Variations of the average Nusselt number on the Marangoni number and Lewis number for $Nr = 0.1$, $Nt = 0.1$, $Nb = 0.1$ (**a**) and thermophoresis parameter for $Le = 1000$, $Nr = 0.1$, $Nb = 0.1$ (**b**)

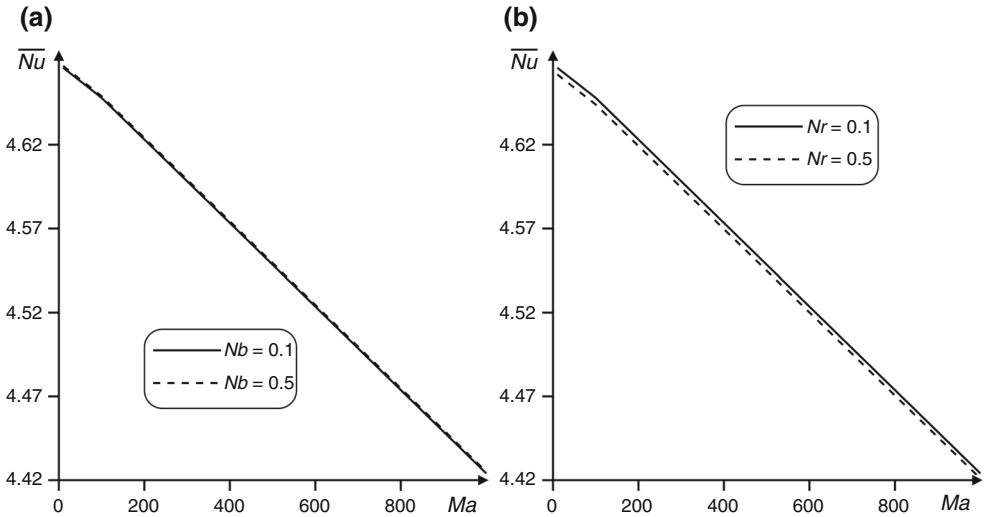

Fig. 6 Variations of the average Nusselt number on the Marangoni number and Brownian diffusion parameter for $Le = 1000$, $Nr = 0.1$, $Nt = 0.1$ (**a**) and buoyancy ratio parameter for $Le = 1000$, $Nb = 0.1$, $Nt = 0.1$ (**b**)

Conclusions

Numerical simulation of buoyancy and thermocapillary-driven convective nanofluid flow and heat transfer inside the cubical cavity with upper free surface using the two-phase nanofluid model has been performed for a wide range of the Marangoni number, Lewis number, thermophoresis parameter, Brownian diffusion parameter and buoyancy ratio parameter. The obtained results illustrate an essential effect of these governing parameters on velocity, temperature and nanoparticles volume fraction patterns as well as average Nusselt number at hot wall. It has been found that a rise of the Marangoni number leads to the heat transfer rate reduction and a formation of addition recirculation near the upper right corner. At the same time, the convective flow intensity decreases with the Marangoni number and weakly increases with the Lewis number, while the growth of latter reflects a diminution of the average Nusselt number. It should be noted that Brownian diffusion parameter does not lead to observable modification of the considered profiles or heat transfer rate.

Acknowledgements This work of Mikhail A. Sheremet was conducted as a government task of the Ministry of Education and Science of the Russian Federation (Project Number 13.6542.2017/6.7). The work of Ioan Pop has been supported from the Grant PN-III-P4-ID-PCE-2016-0036, UEFISCDI, Romania.

References

1. Levich VG. Physicochemical hydrodynamics. Englewood Cliffs: Prentice-Hall; 1962.
2. Sawistowski H. Interfacial phenomena. In: Hanson C, editor. Recent advances in liquid–liquid extraction. Oxford: Pergamon; 1971. p. 293–366.
3. Daniel S, Chaudhury MK, Chen JC. Fast drop movements resulting from the phase change on a gradient surface. Science. 2001;291:633–6.
4. Daniel S, Sircar S, Gliem J, Chaudhury MK. Ratcheting motion of liquid drops on gradient surfaces. Langmuir. 2004;20:4085–92.
5. Colegate DM, Bain CD. Adsorption kinetic in micellar solutions of nonionic surfactant. Phys Rev Lett. 2005;95:198302.
6. Weiss M, Darton CR, Battal T, Bain CD. Surfactant adsorption and Marangoni flow in liquid jets. 3. Modeling in the presence of micellar surfactant. Ind Eng Chem Res 2006;45:2235–48
7. Bahadur P, Yadav PS, Chaurasia K, Leh A, Tadmor R. Chasing drops: following escaper and pursuer drop couple system. J Colloid Interface Sci. 2009;332:455–60.
8. Tadmor R. Marangoni flow revisited. J Colloid Interface Sci. 2009;332:451–4.
9. Magyari E, Chamkha AJ. Exact analytical results for the thermosolutal MHD Marangoni boundary layers. Int J Thermal Sci. 2008;47:848–57.
10. Napolitano LG. Microgravity fluid dynamics. In: 2nd Levitch conference, Washington. 1978.
11. Napolitano LG. Marangoni boundary layers. In: Proceedings of the 3rd European symposium on material science in space, Grenoble, ESA SP-142, 1979.
12. Napolitano LG. Surface and buoyancy driven free convection. Acta Astronaut. 1982;9:199–215.
13. Pop I, Postelnicu A, Grosan T. Thermosolutal Marangoni forced convection boundary layers. Meccanica. 2001;36:555–71.
14. Chamkha AJ, Pop I, Takhar HS. Marangoni mixed convection boundary layerflow. Meccanica. 2006;41:219–32.
15. Al-Mudhaf A, Chamkha AJ. Similarity solutions for MHD thermosolutal Marangoni convection over a flat surface in the presence of heat generation or absorption effects. Heat Mass Transf. 2005;42:112–21.
16. Arifin NM, Nazar R, Pop I. Non-isobaric Marangoni boundary layer flow for Cu, Al_2O_3 and TiO_2 nanoparticles in a water based fluid. Meccanica. 2011;46:833–43.
17. Gollub JP, Benson SV. Many routes to turbulent convection. J Fluid Mech. 1980;100:449–70.
18. Mukutmoni D, Yang KT. Rayleigh-Benard convection in a small aspect ratio enclosure 1. Bifurcation to oscillatory convection, ASME J Heat Transf. 1993;115:360–6.
19. Mukutmoni D, Yang KT. Rayleigh–Benard convection in a small aspect ratio enclosure 2. Bifurcation to chaos. J Heat Transf. 1993;115:367–76.
20. Mukutmoni D, Yang KT. Thermal convection in small enclosures—an atypical bifurcation sequence. Int J Heat Mass Transf. 1995;38:113–26.
21. Bucchignani E, Stella F. Rayleigh–Benard convection in limited domains: part 2—transition to chaos. Numer. Heat Tranf A. 1999;36:17–34.
22. Rahal S, Cerisier P, Abid C. Transition to chaos via the quasi-periodicity and characterization of attractors in confined Benard–Marangoni convection. Eur Phys J B. 2007;59:509–18.
23. Bucchignani E, Mansutti D. Horizontal thermal convection in a shallow cavity: oscillatory regimes and transition to chaos. Int J Numer Methods Heat Fluid Flow. 2000;10:179–95.
24. Bucchignani E, Mansutti D. Horizontal thermocapillary convection of succinonitrile: steady state, instabilities, and transition to chaos. Phys Rev E. 2004;69:056319.
25. Li Y-S, Chen Z-W, Zhan J-M. Double-diffusive Marangoni convection in a rectangular cavity: transition to chaos. Int J Heat Mass Transf. 2010;53:5223–31.
26. Bergman TL. Numerical simulation of double-diffusive Marangoni convection. Phys Fluids. 1986;29:2103–8.
27. Chamkha AJ. Double-diffusive convection in a porous enclosure with cooperating temperature and concentration gradients and heat generation or absorption effects. Numer Heat Transf A. 2002;41:65–87.
28. Chamkha AJ, Grosan T, Pop I. Fully developed free convection of a micropolar fluid in a vertical channel. Int Commun Heat Mass Transf. 2002;29:1119–27.
29. Choi SUS. Enhancing thermal conductivity of fluids with nanoparticles. In: Proceedings of the 1995 ASME international mechanical engineering congress and exposition, FED 231/MD 66; 1995. p. 99–105.
30. Manca O, Jaluria Y, Poulikakos D. Heat transfer in nanofluids. Adv Mech Eng. 2010; Article ID 380826, 2010.
31. Timilsina GR, Kurdgelashvili L, Narbel PA. Solar energy: markets, economics and policies. Renew Sustain Energy Rev. 2012;16:449–65.
32. Routbort J. Argonne national lab. Michellin North America: St. Gobain Corp; 2009.
33. Donzelli G, Cerbino R, Vailati A. Bistable heat transfer in a nanofluid. Phys Rev Lett. 2009;102:104503.
34. Kim SJ, Bang IC, Buongiorno J, Hu LW. Study of pool boiling and critical heat flux enhancement in nanofluids. Bull Polish Acad Sci Tech Sci. 2007,55: 211–16.
35. Das SK, Choi SUS, Yu W, Pradeep Y. Nanofluids: science and technology. New Jersey: Wiley; 2008.
36. Nield DA, Bejan A. Convection in porous media. 4th ed. New York: Springer; 2013.
37. Shenoy A, Sheremet M, Pop I. Convective flow and heat transfer from wavy surfaces: viscous fluids, porous media and nanofluids. New York: CRC Press, Taylor & Francis Group; 2016.
38. Buongiorno J. Convective transport in nanofluids. ASME J Heat Transf. 2006;128:240–50.
39. Buongiorno J, et al. A benchmark study on the thermal conductivity of nanofluids. J Appl Phys. 2009;106:1–14.
40. Kakaç S, Pramuanjaroenkij A. Review of convective heat transfer enhancement with nanofluids. Int J Heat Mass Transf. 2009;52:3187–96.
41. Lee JH, Lee SH, Choi CJ, Jang SP, Choi SUS. A review of thermal conductivity data, mechanics and models for nanofluids. Int J Micro-Nano Scale Transp. 2010;1:269–322.
42. Fan J, Wang L. Review of heat conduction in nanofluids. ASME J Heat Transf. 2011;133:1–14.
43. Mahian O, Kianifar A, Kalogirou SA, Pop I, Wongwises S. A review of the applications of nanofluids in solar energy. Int J Heat Mass Transf. 2013;57:582–94.
44. Sheikholeslami M, Ganji DD. Nanofluid convective heat transfer using semi analytical and numerical approaches: a review. J Taiwan Inst Chem Eng 2016;65(2016):43–77.
45. Nield DA, Kuznetsov AV. Thermal instability in a porous medium layer saturated by a nanofluid: a revised model. Int J Heat Mass Transf. 2014;68:211–4.
46. Nield DA, Kuznetsov AV. The onset of convection in a horizontal nanofluid layer of finite depth: a revised model. Int J Heat Mass Transf. 2014;77:915–8.
47. Kuznetsov AV, Nield DA. Natural convective boundary-layer flow of a nanofluid past a vertical plate. Int J Thermal Sci. 2010;49:243–7.

48. Kuznetsov AV, Nield DA. The Cheng-Minkowycz problem for natural convective boundary layer flow in a porous medium saturated by a nanofluid: a revised model. Int J Heat Mass Transf. 2013;65:682–5.
49. Sheikholeslami M, Chamkha AJ. Influence of Lorentz forces on nanofluid forced convection considering Marangoni convection. J Mol Liq. 2017;225:750–7.
50. Chamkha AJ, Ismael MA. Conjugate heat transfer in a porous cavity filled with nanofluids and heated by a triangular thick wall. Int J Therm Sci. 2013;67:135–51.
51. Zargartalebi H, Ghalambaz M, Noghrehabadi A, Chamkha AJ. Natural convection of a nanofluid in an enclosure with an inclined local thermal non-equilibrium porous fin considering Buongiorno's model. Numer Heat Transf A. 2016;70:432–45.
52. Sheikholeslami M, Chamkha AJ, Rana P, Moradi R. Combined thermophoresis and Brownian motion effects on nanofluid free convection heat transfer in an L-shaped enclosure. Chin J Phys. 2017;55:2356–70.
53. Alsabery AI, Ismael MA, Chamkha AJ, Hashim I. Mixed convection of Al2O3-water nanofluid in a double lid-driven square cavity with a solid inner insert using Buongiorno's two-phase model. Int J Heat Mass Transf. 2018;119:939–61.
54. Alsabery AI, Sheremet MA, Chamkha AJ, Hashim I. Conjugate natural convection of Al_2O_3-water nanofluid in a square cavity with a concentric solid insert using Buongiorno's two-phase model. Int J Mech Sci. 2018;136:200–19.
55. Martyushev SG, Sheremet MA. Conjugate natural convection combined with surface thermal radiation in a three-dimensional enclosure with a heat source. Int J Heat Mass Transf. 2014;73:340–53.
56. Sheremet MA, Pop I, Rahman MM. Three-dimensional natural convection in a porous enclosure filled with a nanofluid using Buongiorno's mathematical model. Int J Heat Mass Transf. 2015;82:396–405.
57. Bondareva NS, Sheremet MA. 3D natural convection melting in a cubical cavity with a heat source. Int J Thermal Sci. 2017;115:43–53.
58. Kolsi L, Oztop HF, Borjini MN, Al-Salem K. Second law analysis in a three dimensional lid-driven cavity. Int Commun Heat Mass Transf 2011;38:1376–83.
59. Maatki C, Kolsi L, Oztop HF, Chamkha A, Borjini MN, Aissia HB, Al-Salem K. Effects of magnetic field on 3D double diffusive convection in a cubic cavity filled with a binary mixture. Int Commun Heat Mass Transf. 2013;49:86–95.
60. Kolsi L, Alrashed AAAA, Al-Salem K, Oztop HF, Borjini MN. Control of natural convection via inclined plate of CNT-water nanofluid in an open sided cubical enclosure under magnetic field. Int J Heat Mass Transf. 2017;111:1007–18.